

Sub-shot-noise emission statistics of a CW-excited single photon source

G. Gavello,¹ G. Petrini,^{1,2} I. Ruo Berchera,² M. Gramegna,² E. Moreva,² P. Traina,²
M. Ziino,¹ M. Genovese,^{2,3} P. Olivero,^{1,3} J. Forneris,^{1,3} and I.P. Degiovanni^{2,3,4}

¹Physics Department - University of Torino - Torino 10025 - Italy

²Istituto Nazionale di Ricerca Metrologica (INRiM) - Torino 10135 - Italy

³Istituto Nazionale di Fisica Nucleare (INFN) - Sezione di Torino - Torino 10125 - Italy

⁴contact: i.degiovanni@inrim.it

Shot noise sets a fundamental limit on the sensitivity of classical optical measurements, with coherent emitters achieving the lowest possible shot-noise level. Emission from sub-Poissonian light provides a pathway to surpass this limit, and single-photon sources provide a natural platform for generating such light. However, it is commonly assumed that continuously excited single-photon sources exhibit Poissonian statistics. In this work, a theoretical model of a continuously driven two-level single-photon source is developed, treating both excitation and radiative decay as stochastic processes. The analysis demonstrates that photon emission can display sub-Poissonian statistics when excitation and decay rates are comparable, showing that continuous excitation does not inherently preclude nonclassical emission. The model is further extended to include finite detection efficiency and detector dead time, illustrating how these practical non-idealities can affect the experimental observation of sub-Poissonian statistics.

I. INTRODUCTION

Optical measurements are fundamentally limited by shot noise, a consequence of the quantized nature of light. In classical imaging, the lowest shot-noise level is achieved using coherent light, which follows Poissonian photon statistics. Light sources with larger intensity fluctuations – such as thermal light, which exhibits super-Poissonian statistics – produce even higher level of noise. Consequently, the Poissonian case sets a strict upper bound on the signal-to-noise ratio achievable in classical imaging. Enhancing measurement precision within this limit requires either increasing optical power or extending acquisition times, approaches that may be impractical in low-light conditions or potentially damaging to sensitive samples.

Quantum imaging, by contrast, offers a way to surpass these classical constraints by exploiting light with nonclassical photon statistics [1–6]. In particular, sub-Poissonian light, where photon-number fluctuations are suppressed below the Poissonian level, can improve measurement precision without increasing the mean photon number. A common implementation involves using twin-beam states [7–10], generated through spontaneous parametric down-conversion or four-wave mixing. In these states, a single pump photon produces two strongly correlated photons: the signal photon, which probes the object, and the idler photon, which serves as a reference. By exploiting their quantum intensity correlations and performing differential detection, correlated fluctuations can be canceled, allowing precision beyond the classical shot-noise limit [11–14]. While progresses have been made towards applicability with twin beam strategies [15, 16], to achieve high spatial resolution imaging is still a challenge due to the intrinsic coherence size of quantum correlations and the need of preserving through high numerical aperture optical system.

An alternative approach involves using single-photon sources (SPSs), which provide a more direct path to sub-Poissonian statistics. Ideally, a SPS emits exactly one photon at a time

on demand, with each emitted photon being identical and indistinguishable from the others [17]. Various platforms have been developed to realize such emitters. Solid-state systems, such as diamond color centers [18, 19] and semiconductor quantum dots [20], combine high brightness with on-chip integration [21], with diamond centers operable at room temperature. Atomic and ionic systems, including trapped atoms or ions [22], deliver extremely pure single-photon emission with well-defined quantum states, though they typically require complex trapping and cooling. Emerging platforms, such as defect-engineered non-diamond crystals [23, 24] and two-dimensional materials such as transition metal dichalcogenides [25], further expand the options for scalable and versatile SPS implementation. Despite their potential, conventional assumptions assert that SPSs under continuous-wave excitation exhibit Poissonian statistics, rendering them unsuitable for sub-shot-noise imaging. In this work, theoretical modeling of a continuously driven two-level SPS demonstrates that, under specific conditions, such systems can exhibit sub-Poissonian photon statistics. This indicates that continuous excitation does not inherently preclude nonclassical emission. Based on this finding, the feasibility of experimental validation is examined, accounting for the influence of realistic non-idealities on the detection of sub-Poissonian behavior.

II. MODEL

The system addressed in this model is a two-level SPS, initially prepared in its ground state and subsequently exposed to continuous optical excitation. Upon absorption of a pump photon, the SPS is promoted to its excited state and then relaxes back to the ground level via photon emission. Considered separately, photon absorption and emission are modeled as Poissonian processes. Absorption occurs at a rate μ_1 directly proportional to the excitation power P (i.e. $\mu_1 = \alpha P$), whereas emission occurs at a rate $\mu_2 = 1/\tau$, where τ is the characteristic radiative lifetime of the SPS

excited state. Consequently, assuming that the optical pump is activated at $t = 0$, the probability density function (PDF) describing the absorption of a photon is:

$$f_{\text{abs}}(t) = \mu_1 e^{-\mu_1 t} \theta(t), \quad (1)$$

with θ being the Heaviside function. Similarly, the PDF describing the emission of a photon, assuming a pump photon was absorbed at $t = 0$ is:

$$f_{\text{em}}(t) = \mu_2 e^{-\mu_2 t} \theta(t). \quad (2)$$

Within this framework, assuming that each subsequent absorption–emission cycle is independent of the others, the PDF for the SPS to emit a photon given the optical pump activated at $t = 0$ can be expressed as the following convolution of the two PDFs presented in eqs.1 and 2:

$$f(t) = \int dt' dt'' f_{\text{abs}}(t') f_{\text{em}}(t'') \delta(t - t' - t''),$$

whose analytical expression is:

$$f(t) = \frac{\mu_1 \mu_2}{\mu_1 - \mu_2} (e^{-\mu_2 t} - e^{-\mu_1 t}) \theta(t). \quad (3)$$

From the expression above, it is evident that in the limiting cases where $\mu_1 \gg \mu_2$ or $\mu_1 \ll \mu_2$, the statistics of the combined absorption–emission process is poissonian, reflecting the fact that the dominant process itself follows Poisson statistics. In contrast, in the intermediate regime the behavior is not immediately apparent and the moments of the corresponding statistical distribution must therefore be explicitly derived. In principle, this would involve determining the probability $P_T(n)$ that the SPS emits n photons within a time interval T and subsequently calculating the moments from $P_T(n)$. However, this approach is not practical here, as it would require evaluating a n -fold convolution of PDFs of the form given in eq. 3, each evaluated at a different time (see appendix A). A more convenient approach is to introduce the probability generating function (PGF).

For n , the number of photons emitted by the SPS during the time interval T , the PGF is defined as $G(T, \xi) = \sum_{n=0}^{\infty} P_T(n) \xi^n$. This function is a powerful tool, as it enables the moments of the photon statistics to be straightforwardly derived from its analytical expression via simple differentiation with respect to ξ . Although the convolution issue formally persists – since $P_T(n)$ corresponds to a n -fold convolution of PDFs as discussed in appendix A – it can be overcome by considering the Laplace transform of the PGF: $\tilde{G}(s, \xi)$. As shown in Appendix B, this quantity takes the form

$$\tilde{G}(s, \xi) = \frac{1}{s} \frac{1 - \tilde{f}(s)}{1 - \xi \tilde{f}(s)}, \quad (4)$$

where $\tilde{f}(s)$ is the Laplace transform of a single PDF of the type given in eq. 3. Explicitly:

$$\tilde{f}(s) = \frac{\mu_1 \mu_2}{(\mu_1 + s)(\mu_2 + s)}. \quad (5)$$

From eq. 4, the moments of the photon statistics are obtained by differentiating $\tilde{G}(s, \xi)$ with respect to ξ and then applying the inverse Laplace transform to return to the time domain. For instance, the mean number of photons emitted by the SPS over T , denoted $\langle n \rangle_T$, is obtained as:

$$\langle n \rangle_T = \mathcal{L}^{-1} \left[\frac{d}{d\xi} \tilde{G}(s, \xi) \Big|_{\xi=1} \right],$$

where \mathcal{L}^{-1} represents the inverse Laplace transform operation. Similarly, the variance $\text{Var}[n]_T$ is obtained as $\text{Var}[n]_T = \langle n(n-1) \rangle_T + \langle n \rangle_T - \langle n \rangle_T^2$, with $\langle n(n-1) \rangle_T$ calculated via

$$\langle n(n-1) \rangle_T = \mathcal{L}^{-1} \left[\frac{d^2}{d\xi^2} \tilde{G}(s, \xi) \Big|_{\xi=1} \right].$$

The quantities $\langle n \rangle_T$ and $\text{Var}[n]_T$ are obtained following the procedure described above, with their general expressions reported in Appendix C. Only their asymptotic forms for long times ($T \rightarrow \infty$) are considered here, as photon counting is usually carried out over macroscopic time windows ranging from ms to s, which can be treated as effectively infinite compared to the ns/ μ s relaxation times typical of existing SPSs [26, 27]. In this limit, the quantities are given by:

$$\langle n \rangle_{\infty} = \frac{\mu_1 \mu_2}{(\mu_1 + \mu_2)} T \quad (6)$$

$$\text{Var}[n]_{\infty} = \frac{\mu_1^2 + \mu_2^2}{(\mu_1 + \mu_2)^2} \cdot \langle n \rangle_{\infty} \quad (7)$$

At this stage, it is convenient to introduce the quantity $\xi_{\infty} = \text{Var}[n]_{\infty} / \langle n \rangle_{\infty}$ which provides a direct measure of the emission statistics. Figure 1 shows this ratio as a function of μ_1 / μ_2 .

In agreement with the calculations above, the statistics is poissonian ($\xi_{\infty} = 1$) when $\mu_1 \gg \mu_2$ or $\mu_1 \ll \mu_2$. Interestingly, in the intermediate regime, where no prior information was available, the emission statistics turns out to be sub-poissonian ($\xi_{\infty} < 1$), reaching $\xi_{\infty} = 1/2$ for $\mu_1 = \mu_2$.

To complete the characterization of the SPS, its asymptotic emission intensity is directly obtained from eq.6 as the mean number of photons emitted over the macroscopic measurement time T . Using the relationships linking μ_1 and μ_2 to the pump power P and the characteristic lifetime τ of the source, the photon rate is expressed as:

$$I_{\infty} = \frac{1}{\tau} \frac{\alpha P}{\alpha P + 1/\tau}$$

which is commonly rewritten in the familiar saturation form:

$$I_{\infty} = I_{\text{sat}} \frac{P}{P + P_{\text{sat}}}$$

where $I_{\text{sat}} = \tau^{-1}$ is the maximum photon emission rate of the SPS, and the saturation power is $P_{\text{sat}} = (\tau \alpha)^{-1}$.

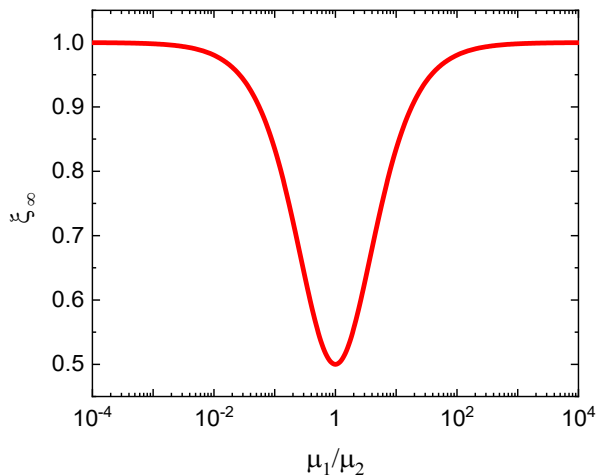


FIG. 1. Plot of the quantity ξ_∞ , defined as the ratio of the variance to the mean number of emitted photons by a continuously excited single-photon source in the large-time limit, as a function of the ratio μ_1/μ_2 .

III. DISCUSSION

The identification of a regime in which a continuously excited SPS exhibits sub-Poissonian emission is particularly significant, as it points to the possibility of achieving sub-shot-noise imaging with these systems. Any realistic evaluation of this potential, however, requires experimental verification of the regime predicted. This would involve measuring ξ_∞ at different laser powers to span different values of μ_1 , while μ_2 remains fixed by the choice of SPS. Observing a minimum in ξ_∞ when $\mu_1 = \mu_2$ would thus indicate the sub-Poissonian nature of the continuously excited SPS.

However, it is essential to remark that practical photon-counting measurements are affected by inefficiencies at the collection level. As a result, the statistics of the detected photons may differ from the intrinsic emission statistics of the SPS, causing the observed behavior to deviate from the idealized model described above. To address this, the model is extended to analyze how non-idealities influence the outcome and to identify the conditions under which a sub-Poissonian signature can still be observed.

Initially, the focus is on optical losses that can be quantified by a detection efficiency η , defined as the ratio of photons detected to photons emitted by the SPS. This parameter can encompass a variety of loss mechanisms, including imperfect photon extraction from the SPS, suboptimal coupling between the source and the detection apparatus, the finite efficiency of the detector itself. Furthermore, η can be extended to account for the fact that in real SPSs, not every photon absorbed leads to a radiative emission [28], as alternative relaxation pathways may exist.

Within this framework, if the SPS emits n photons during a measurement interval T , only a fraction η is registered by the measurement system. Consequently, the detection PDF is not simply the convolution of n copies of the SPS $f(t)$

from eq. 3, denoted by $f_n(t)$ (see Appendix A). To illustrate this point, consider the scenario in which the n -th emitted photon is the first one to be detected, while the preceding $n-1$ photons were missed due to imperfect detection efficiency. In this case, the corresponding PDF is given by $\eta(1-\eta)^{n-1}f_n(t)$.

Generalizing this idea, the total detection PDF must account for all possible scenarios in which an arbitrary number of photons are lost before a successful detection occurs. This leads to:

$$f_\eta(t) = \sum_{n=1}^{\infty} \eta(1-\eta)^{n-1}f_n(t), \quad (8)$$

whose Laplace transform, as shown in Appendix D, is given by:

$$\tilde{f}_\eta(s) = \eta \frac{\tilde{f}(s)}{1 - (1-\eta)\tilde{f}(s)}. \quad (9)$$

Once this expression is obtained, the statistics at the detection stage is evaluated by following the same procedure previously adopted. Specifically, the Laplace transform of the PGF is computed by replacing $\tilde{f}(s)$ in eq. 4 with the modified function $\tilde{f}_\eta(s)$, thereby explicitly accounting for optical losses. From the resulting expression, the mean number of detected photons and their variance in the presence of losses, $\langle n_\eta \rangle_T$ and $\text{Var}[n_\eta]_T$, are determined through differentiation with respect to the generating variable, followed by inverse Laplace transformation. Restricting the attention to the large-time limit ($T \rightarrow \infty$) as done before, their asymptotic expressions are given by:

$$\langle n_\eta \rangle_\infty = \eta \frac{\mu_1 \mu_2}{(\mu_1 + \mu_2)} T$$

$$\text{Var}[n_\eta]_\infty = \frac{\mu_1^2 + 2(1-\eta)\mu_1\mu_2 + \mu_2^2}{(\mu_1 + \mu_2)^2} \cdot \langle n_\eta \rangle_\infty$$

In this case as well, it is convenient to compute the ratio between these former quantities, namely $\xi_\infty(\eta) = \text{Var}[n_\eta]_\infty / \langle n_\eta \rangle_\infty$. Figure 2 displays this quantity as a function of μ_1/μ_2 for three different detection efficiencies: $\eta = 1$ (ideal reference case, red solid line), $\eta = 0.5$ (green solid line), and $\eta = 0.1$ (blue solid line). When compared with the ideal scenario, it becomes clear that detection losses produce a uniform vertical rescaling of the curve. Although the shape and the position of the minimum remain unaffected, its depth is progressively reduced as the efficiency decreases. Thus, the nonclassical signature encoded in the suppression of ξ_∞ at $\mu_1 = \mu_2$ becomes less pronounced for smaller η . Experimentally, this means that tuning μ_1 by sweeping the pump power (with μ_2 fixed by the selected SPS) will yield a flatter profile than in the lossless case. For very low efficiencies, the contrast of the minimum may approach the level of instrumental noise, increasing the risk that the sub-Poissonian nature of the SPS becomes partially or completely obscured in realistic measurements.

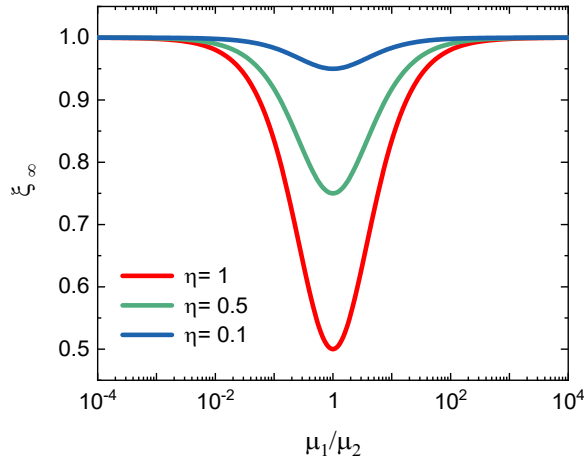


FIG. 2. Plot of the quantity $\xi_\infty(\eta)$, defined as the ratio of the variance to the mean number of emitted photons by a continuously excited single-photon source in the large-time limit in the presence of optical losses. Losses are quantified by the detection efficiency η . The ratio is displayed as a function of μ_1/μ_2 , with each colored curve corresponding to a different η value indicated in the legend.

Attention is now directed to another non-ideality affecting the detection process that must be accounted for in a realistic discussion, namely the finite dead time of detectors. Depending on the underlying physical mechanisms, detectors are generally classified as either paralyzable or non-paralyzable. In the non-paralyzable case, once an event is registered, the system becomes inactive for a fixed interval – referred to as the dead time and denoted by D . During this period, any subsequent incoming events are simply ignored and do not extend the duration of the inactive state. By contrast, in paralyzable detectors, events occurring within the dead time prolong its duration. Restricting the discussion to non-paralyzable systems – such as single-photon avalanche diodes (SPADs) operated in Geiger mode with active quenching circuits, which constitute the most widely used commercial solutions for single-photon detection [29] – the detected event rate ν_{out} is thus related to the true incoming rate ν_{in} by:

$$\nu_{out} = \frac{\nu_{in}}{1 + D \nu_{in}}.$$

This relation indicates that the measured rate is reduced relative to the true rate, with the reduction acting effectively as an efficiency factor that depends on both the dead time D and the event rate itself. Consequently, the detection PDF derived in eq. 8 no longer accurately represents the statistics in the presence of a non-zero detector dead time. In this case, the correct PDF must instead be written as $f_{D,\eta}(t) = A f_\eta(t) \theta(t - D)$ so that, given a detection event at $t = 0$, the distribution remains zero throughout the detector recovery interval and, after the dead time D has elapsed, becomes proportional to $f_\eta(t)$. The constant A ensures proper normalization of the modified PDF. Enforcing

this normalization condition yields the expression:

$$f_{D,\eta}(t) = \frac{e^{-\frac{\mu_m t}{2}} - e^{-\frac{\mu_p t}{2}}}{2 \left(\frac{e^{-\frac{\mu_m D}{2}} - e^{-\frac{\mu_p D}{2}}}{\mu_m} - \frac{e^{-\frac{\mu_p D}{2}} - e^{-\frac{\mu_m D}{2}}}{\mu_p} \right)} \theta(t - D)$$

with $\mu_p = (\mu_1 + \mu_2) + \sqrt{(\mu_1 + \mu_2)^2 - 4\eta\mu_1\mu_2}$ and $\mu_m = (\mu_1 + \mu_2) - \sqrt{(\mu_1 + \mu_2)^2 - 4\eta\mu_1\mu_2}$. Following the same procedure as before, the Laplace transform of the PDF just obtained is computed, resulting in:

$$\tilde{f}_{D,\eta}(s) = \frac{\mu_p \mu_m \left(\frac{2e^{-\frac{1}{2}(2s+\mu_m)D}}{2s+\mu_m} - \frac{2e^{-\frac{1}{2}(2s+\mu_p)D}}{2s+\mu_p} \right)}{2 \left(\mu_p e^{-\frac{\mu_m D}{2}} - \mu_m e^{-\frac{\mu_p D}{2}} \right)}.$$

The Laplace transform of the PGF is then computed by replacing $\tilde{f}(s)$ in eq. 4 with the modified function $\tilde{f}_{D,\eta}(s)$, thereby explicitly accounting for both optical losses and dead time. From this expression, the next step would involve determining the mean number of detected photons and their variance, $\langle n_{D,\eta} \rangle_T$ and $\text{Var}[n_{D,\eta}]_T$, through differentiation with respect to the generating variable, followed by inverse Laplace transformation. In this case, however, the inverse Laplace transform does not yield a closed-form analytical expression as it did for zero dead time. This difficulty can nevertheless be circumvented, since the analysis only requires the asymptotic limit for long acquisition times ($T \rightarrow \infty$), for which an analytical function can still be derived. Concretely, this is achieved by retaining only the terms in the series expansion of the Laplace-transformed PGF whose order is negative and then performing the inverse transformation. This procedure is justified by the fact that the limit $T \rightarrow \infty$ in the time domain corresponds to $s \rightarrow 0$ in the Laplace one. Due to the length and complexity of the resulting expressions, the explicit forms of $\langle n_{D,\eta} \rangle_\infty$ and $\text{Var}[n_{D,\eta}]_\infty$ are not reported here. Instead, their ratio in the asymptotic limit, defined as $\xi_\infty(D, \eta) = \text{Var}[n_{D,\eta}]_\infty / \langle n_{D,\eta} \rangle_\infty$, is presented in figure 3. Since the impact of optical losses has already been examined, $\xi_\infty(D, \eta)$ is evaluated at a fixed optical efficiency $\eta = 0.5$. The dead time is expressed in units of the characteristic lifetime τ of the SPS and is varied from $D = 0$ s (dark blue solid line) to $D = \tau$ (red solid line).

Unlike the previous case, a finite dead time has a more surprising impact on ξ_∞ , progressively distorting the curve as the dead time D increases. Even at a relatively short dead time of $D = 0.1\tau$ (solid light blue line), a clear asymmetry emerges: the plateau at $\mu_1 \gg \mu_2$ drops below 1, whereas the plateau at $\mu_2 \gg \mu_1$ remains largely unaffected. This asymmetry can be consistently interpreted as an artificial sub-Poissonian signature induced by the non-paralyzable dead time. Indeed, in the regime $\mu_1 \ll \mu_2$, the dynamics is dominated by a slow absorption time, which effectively limits the counting rate. As a result, detection events are sufficiently sparse that the dead time plays a negligible role, and the system reproduces the behavior expected in the zero-dead-time limit. Conversely, when $\mu_1 \gg \mu_2$, the intrinsic event rate is significantly higher, and the dead time

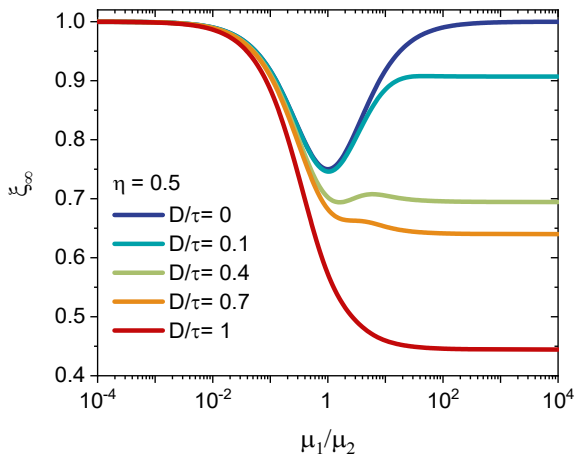


FIG. 3. Plot of the quantity $\xi_\infty(D, \eta)$, defined as the ratio of the variance to the mean number of emitted photons by a continuously excited single-photon source in the large-time limit in the presence of optical losses and finite detector dead time D . The ratio is displayed as a function of μ_1/μ_2 , with each colored curve corresponding to a different D value indicated in the legend, expressed in unit of the characteristic lifetime τ of the single-photon source. Since the impact of optical losses has already been considered, all curves are calculated for a fixed optical efficiency: $\eta = 0.5$.

actively suppresses closely spaced detection events. This leads to an apparent sub-poissonian character and, consequently, to a lowering of the ξ_∞ plateau. As the dead time increases further, the asymmetry becomes more pronounced: at around $D = 0.5\tau$ (green solid line), the position of the minimum shifts slightly away from $\mu_1 = \mu_2$. When the dead time approaches the SPS lifetime ($D = \tau$, red solid line), the minimum disappears entirely, and the measurement is completely dominated by the fake sub-poissonian behavior induced by the detector dead time, confirming this interpretation. From an experimental standpoint, this highlights the importance of using detectors with a dead time shorter than the lifetime of the SPS under investigation. Otherwise, the sub-poissonian character of the source may be confused with non-idealities of the detection system.

IV. CONCLUSIONS

In this work, a comprehensive theoretical model was developed for a continuously excited two-level single-photon source, treating excitation and radiative decay as stochastic processes within a unified description. By employing the probability generating function and its Laplace-transform properties, explicit expressions for the long-time mean photon number and variance were obtained, providing a direct characterization of the emission statistics.

The analysis shows that the single-photon source exhibits Poissonian statistics when one of the underlying dynamical processes dominates. When excitation and radiative decay occur on comparable time scales, the photon statistics

become sub-Poissonian, demonstrating that continuous excitation does not preclude intrinsically nonclassical emission. The framework was further extended to include realistic detection effects. Limited collection efficiency reduces the visibility of the nonclassical signature without fundamentally altering its structure, whereas finite detector dead time can significantly distort the statistics and may induce a fake sub-Poissonian character.

Overall, the theoretical framework developed here not only elucidates the statistical properties of continuously excited single-photon sources but also provides practical guidance for experimental verification and the development of quantum-enhanced technologies.

APPENDIX A

As outlined in the main text, $P_T(n)$ involves a n -fold convolution of PDFs of the form given in eq. 3, which renders the direct calculation of the corresponding statistical moments impractical. The origin of this n -fold convolution is clarified here. Specifically, $P_T(n)$ can be expressed in terms of the auxiliary quantity $K_n(T)$, defined as the probability that the n -th photon emitted by the SPS occurs within the time interval $[0, T]$. From this definition, this quantity is given by the integral over $[0, T]$ of the convolution of n copies of eq. 3:

$$K_n(T) = \int_0^T f(t_1) \dots f(t_n) \delta(t - t_1 \dots - t_n) dt dt_1 \dots dt_n$$

which can be rewritten more compactly as

$$K_n(T) = \int_0^T f_n(t) dt \quad (10)$$

where $t = \sum_{i=1}^n t_i$ arises from the action of the Dirac delta function, and $f_n(t)$ denotes the n -fold convolution of $f(t)$.

Equivalently, $K_n(T)$ can be interpreted as the cumulative probability of having at least n photons emitted within the same interval. This leads to the relation

$$K_n(T) = \sum_{n'=n}^{\infty} P_T(n')$$

from which, by straightforward manipulation, one obtains:

$$P_T(n) = K_n(T) - K_{n+1}(T) \quad (11)$$

This relation explains the appearance of the n -fold convolution of PDFs in the expression for $P_T(n)$.

APPENDIX B

As mentioned in the main text, it is advantageous to work with the Laplace transform of the PGF $G(T, \xi)$, as its expression contains only a single PDF of the form given in eq. 3,

rather than a convolution of n PDFs. A formal proof of this result is provided here.

The PGF $G(T, \xi)$, defined in the main text in terms of $P_T(n)$, is first rewritten as a function of the quantity $K_n(T)$, introduced in Appendix B, using the relation in eq. 11. This yields:

$$G(T, \xi) = 1 + \sum_{n=1}^{\infty} K_n(t) (\xi - 1) \xi^{n-1}$$

The Laplace transform of $G(T, \xi)$ with respect to T is then evaluated. Substitution of the expression for $K_n(T)$ from eq. 10, followed by straightforward algebraic manipulations, yields

$$\tilde{G}(s, \xi) = \frac{1}{s} + \sum_{n=1}^{\infty} \tilde{f}_n(s) (\xi - 1) \xi^{n-1}$$

At this stage, the convolution theorem is invoked, according to which the Laplace transform of a n -fold convolution equals the product of the n Laplace transforms. Consequently, $\tilde{f}_n(s) = (\tilde{f}(s))^n$. Substituting this result into the expression for $\tilde{G}(s, \xi)$ and carrying out elementary manipulations yields:

$$\tilde{G}(s, \xi) = \frac{1}{s} \left\{ 1 + (\xi - 1) \tilde{f}(s) \sum_{m=0}^{\infty} (\xi \tilde{f}(s))^m \right\}$$

The summation in the above equation is a geometric series and admits a closed-form evaluation. Inserting this result yields the expression presented in eq. 4.

APPENDIX C

For completeness, the general expressions for the mean number of emitted photons and their variance – derived from the PGF of a SPS under continuous-wave laser excitation and assuming ideal collection conditions – are given by:

$$\langle n \rangle_T = \frac{\mu_1 \mu_2}{(\mu_1 + \mu_2)^2} (e^{-(\mu_1 + \mu_2)T} + (\mu_1 + \mu_2)T - 1)$$

$$\begin{aligned} \text{Var}[n]_T = & \frac{\mu_1 \mu_2}{(\mu_1 + \mu_2)^4} e^{-2T(\mu_1 + \mu_2)} \{-\mu_1 \mu_2 + e^{2T(\mu_1 + \mu_2)} [T\mu_1^3 + \\ & + (\mu_1^2 + \mu_2^2)(-1 + T\mu_2) + \mu_1 \mu_2(3 + T\mu_2)] + \\ & + e^{T(\mu_1 + \mu_2)} [\mu_2^2 + \mu_1^2(1 - 4T\mu_2) - 2\mu_1 \mu_2(1 + \\ & + 2T\mu_2)]\} \end{aligned}$$

These expressions in the long-time limit ($T \rightarrow \infty$) return eqs. 6,7.

APPENDIX D

This section presents the transformation of eq. 8 into eq. 9. Using the property from Appendix B that the Laplace transform of an n -fold convolution equals the product of the

individual Laplace transforms, one has: $\tilde{f}_n(s) = (\tilde{f}(s))^n$. Accordingly, eq. 8 can be rewritten as:

$$\tilde{f}_\eta(s) = \sum_{n=1}^{\infty} (1 - \eta)^{n-1} \eta (\tilde{f}(s))^n.$$

Through an appropriate shift of the summation index, the series can be expressed as a geometric series:

$$\tilde{f}_\eta(s) = \eta f(s) \sum_{n=0}^{\infty} (1 - \eta)^n (\tilde{f}(s))^n.$$

Replacing the series with its closed-form expression results in the eq. 9 presented in the main text.

AUTHORS CONTRIBUTION

I.P.D., with the support of G.G. and G.P. developed the theoretical model that has been extensively and systematically analysed and discussed by I.R.B., M.G., E.M., P.T., M.Z., M.G., P.O., J.F. The manuscript was prepared with inputs by all the authors.

ACKNOWLEDGMENTS

The results presented in this article had been achieved also in the context of the following projects: QU-TEST which had received funding from the European Union's Horizon Europe under the grant agreement number 101113901; PROMISE which had received funding from the European Union's Horizon Europe under the grant agreement number 101189611; DIREQT, which has received funding from the Chips Joint Undertaking (Chips JU) under grant agreement No [Project Number]; the experiment QUERIS funded by the 5th National Commission of the Italian National Institute for Nuclear Physics (INFN). This work was also funded by the project 23NRM04 NoQTeS, which received funding from the European Partnership on Metrology, co-financed from the European Union's Horizon Europe Research and Innovation Programme and by the Participating States.

REFERENCES

- [1] D. Gatto Monticone, K. Katamadze, P. Traina, E. Moreva, J. Forneris, I. Ruo-Berchera, P. Olivero, I. P. Degiovanni, G. Brida, and M. Genovese, Beating the abbe diffraction limit in confocal microscopy via nonclassical photon statistics, *Phys. Rev. Lett.* **113**, 143602 (2014).
- [2] O. Schwartz and D. Oron, Improved resolution in fluorescence microscopy using quantum correlation, *Phys.Rev. A* **85**, 033812 (2012).
- [3] R. Tenne, U. Rossman, B. Rephael, Y. Israel, A. Krupinski-Ptaszek, R. Lapkiewicz, Y. Silberberg, and D. Oron, Super-resolution enhancement by quantum image scanning microscopy, *Nature Photonics* **13**, 116 (2019).

- [4] I. R. Berchera and I. P. Degiovanni, Quantum imaging with sub-poissonian light: challenges and perspectives in optical metrology, *Metrologia* **56**, 024001 (2019).
- [5] M. Genovese, Real applications of quantum imaging, *Journal of Optics* **18**, 073002 (2016).
- [6] F. Picariello, E. Losero, S. Ditalia Tchernij, P. Boucher, M. Genovese, I. Ruo-Berchera, and I. P. Degiovanni, Quantum super-resolution microscopy by photon statistics and structured light, *Optica* **12**, 490 (2025).
- [7] E. Brambilla, L. Caspani, O. Jedrkiewicz, L. Lugiato, and A. Gatti, High-sensitivity imaging with multi-mode twin beams, *Phys. Rev. A* **77**, 053807 (2008).
- [8] G. Brida, M. Genovese, and I. Ruo Berchera, Experimental realization of sub-shot-noise quantum imaging, *Nat. Photon.* **4**, 227 (2010).
- [9] G. Brida, M. Genovese, and I. Ruo Berchera, Experimental quantum imaging exploiting multimode spatial correlation of twin beams, *Phys. Rev. A* **83**, 033811 (2011).
- [10] G. Ortolano, A. Paniate, P. Boucher, C. Napoli, S. Soman, S. F. Pereira, I. Ruo-Berchera, and M. Genovese, Quantum enhanced non-interferometric quantitative phase imaging, *Light: Science & Applications* **12**, 171 (2023).
- [11] N. Samantaray, I. Ruo-Berchera, A. Meda, and M. Genovese, Realization of the first sub-shot-noise wide field microscope, *Light: Sci. Appl.* **6**, e17005 (2017).
- [12] G. Ortolano, C. Napoli, C. Harney, S. Pirandola, G. Leonetti, P. Boucher, E. Losero, M. Genovese, and I. Ruo-Berchera, Quantum-enhanced pattern recognition, *Phys. Rev. Applied* **20**, 024072 (2023).
- [13] J. Sabines-Chesterking, A. R. McMillan, P. A. Moreau, S. K. Joshi, S. Knauer, E. Johnston, J. G. Rarity, and J. C. F. Matthews, Twin-beam sub-shot-noise raster scanning microscope, *Opt. Express* **27**, 30810 (2019).
- [14] J. Wang, R. L. d. M. Filho, G. S. Agarwal, and L. Davidovich, Quantum advantage of time-reversed ancilla based metrology of absorption parameters, *Phys. Rev. Res.* **6**, 013034 (2024).
- [15] I. Ruo-Berchera, A. Meda, E. Losero, A. Avella, N. Samantaray, and M. Genovese, Improving resolution-sensitivity trade off in sub-shot noise quantum imaging, *Applied Physics Letters* **116**, 214001 (2020).
- [16] A. Paniate, O. Giuseppe, S. Soman, M. Genovese, and I. Ruo-Berchera, High-resolution quantum-enhanced phase imaging of cells, *Optica* **13**, 375 (2026).
- [17] B. Lounis and M. Orrit, Single-photon sources, *Rep. Prog. Phys.* **68**, 1129 (2005).
- [18] D. Gatto Monticone, P. Traina, E. Moreva, J. Forneris, P. Olivero, I. P. Degiovanni, F. Taccetti, L. Giuntini, G. Brida, G. Amato, and M. Genovese, Native nir-emitting single colour centres in cvd diamond, *New Journal of Physics* **16**, 053005 (2014).
- [19] E. Corte, G. Andrini, E. Nieto Hernández, V. Pugliese, Â. Costa, G. Magchiels, J. Moens, S. M. Tunhuma, R. Villarreal, L. M. Pereira, *et al.*, Magnesium-vacancy optical centers in diamond, *ACS Photonics* **10**, 101 (2022).
- [20] B. Costa, B. Scaparra, X. Wei, H. Riedl, G. Koblmüller, E. Zallo, J. J. Finley, L. Hanschke, and K. Müller, Quantum dots on gaas substrates as integration-ready high-performance single-photon sources at telecommunication wavelengths, *Phys. Rev. Appl.* **25**, L011002 (2026).
- [21] K. J. Palm, M. Dong, D. A. Golter, G. Clark, M. Zimmermann, K. C. Chen, L. Li, A. Messen, A. J. Leenheer, D. Dominguez, *et al.*, Modular chip-integrated photonic control of artificial atoms in diamond waveguides, *Optica* **10**, 634 (2023).
- [22] D. B. Higginbottom, L. Slodička, G. Araneda, L. Lachman, R. Filip, M. Hennrich, and R. Blatt, Pure single photons from a trapped atom source, *New J. Phys.* **18**, 093038 (2016).
- [23] G. Grosso, H. Moon, B. Lienhard, S. Ali, D. K. Efetov, M. M. Furchi, P. Jarillo-Herrero, M. J. Ford, I. Aharonovich, and D. Englund, Tunable and high-purity room temperature single-photon emission from atomic defects in hexagonal boron nitride, *Nat. commun.* **8**, 1 (2017).
- [24] M. Radulaski, M. Widmann, M. Niethammer, J. L. Zhang, S.-Y. Lee, T. Rendler, K. G. Lagoudakis, N. T. Son, E. Janzen, T. Ohshima, *et al.*, Scalable quantum photonics with single color centers in silicon carbide, *Nano lett.* **17**, 1782 (2017).
- [25] K. Parto, S. I. Azzam, K. Banerjee, and G. Moody, Defect and strain engineering of monolayer wse₂ enables site-controlled single-photon emission up to 150 k, *Nat. commun.* **12**, 3585 (2021).
- [26] A. Sipahigil, K. D. Jahnke, L. J. Rogers, T. Teraji, J. Isoya, A. S. Zibrov, F. Jelezko, and M. D. Lukin, Indistinguishable photons from separated silicon-vacancy centers in diamond, *Phys. Rev. Lett.* **113**, 113602 (2014).
- [27] J. Stortebom, P. Dolan, S. Castelletto, X. Li, and M. Gu, Lifetime investigation of single nitrogen vacancy centres in nanodiamonds, *Opt. Express* **23**, 11327 (2015).
- [28] M. Nguyen, N. Nikolay, C. Bradac, M. Kianinia, E. A. Ekimov, N. Mendelson, O. Benson, and I. Aharonovich, Photodynamics and quantum efficiency of germanium vacancy color centers in diamond, *Adv. Photon.* **1**, 066002 (2019).
- [29] H. Georgieva, A. Meda, S. M. Raupach, H. Hofer, M. Gramegna, I. P. Degiovanni, M. Genovese, M. López, and S. Kück, Detection of ultra-weak laser pulses by free-running single-photon detectors: modeling dead time and dark counts effects, *Appl. Phys. Lett.* **118**, 10.1063/5.0046014 (2021).